Identification of brain-like functional information architectures in embryonic tissue of *Xenopus laevis*.

Thomas F. Varley,[1,2,*] Vaibhav P. Pai,[3,*] Caitlin Grasso,[2]
Jeantine Lunshof,[4,5] Michael Levin,[3] and Josh Bongard[1,2]

[1] *Vermont Complex Systems Center, University of Vermont, Burlington, VT*
[2] *Department of Computer Science, University of Vermont, Burlington, VT*[†]
[3] *Allen Discovery Institute, Tufts University, Medford, MA*
[4] *Wyss Institute for Biologically Inspired Engineering at Harvard, Boston, MA*
[5] *Department of Genetics, Harvard Medical School, Boston, MA, USA*

(Dated: December 5, 2024)

Abstract

Understanding how populations of cells collectively coordinate activity to produce the complex structures and behaviors that characterize multicellular organisms is a fundamental issue in modern biology. Here we show how mathematical techniques from complex systems science and multivariate information theory can provide a rigorous framework for inferring the structure of collective organization in non-neural tissue. Many of these techniques were developed and refined in the context of theoretical neuroscience, a field well-used to the problem of inferring coordinated activity in high-dimensional data. In neuroscience, these statistics (functional connectivity network structure, modularity, higher-order information, etc) have been found to be altered during different cognitive, clinical, or behavioral states and are generally thought to be informative about the underlying dynamics linking biology to cognition. Here we show that these same patterns of coordinated activity are also present in the aneural tissues of evolutionarily distant biological systems: preparations of self-motile embryonic *Xenopus* tissue (colloquially known as "basal Xenobots"). When analyzing calcium recordings from basal Xenobots and comparing them to fMRI recordings from a sample of adult human brains, we find that the bots have a "brain-like" functional information architecture, complete with positive and negative functional connections, meso-scale communities, higher-order redundant and synergistic interactions, and integrated information that is "greater than the sum of its parts". By comparing each recording (brain and bot) to a personalized null model that preserves all first-order statistical structures (autocorrelation, frequency spectrum, etc.) while disrupting all higher-order interactions, we show that these are genuine higher order interactions and not trivially reducible to lower-order features of the data. These similarities suggest that such patterns of activity and information structures either: arose independently in these two systems epithelial constructs and brains, are epiphenomenological byproducts of other dynamics conserved across vastly different configurations of life; or somehow directly support adaptive behavior across diverse living systems.

Keywords: Developmental biology, neuroscience, functional connectivity, emergence, synergy, multivariate information theory.

I. INTRODUCTION

One of the hallmarks of biological systems is what cybernetician Warren Weaver called "organized complexity" [1]. In contrast to simple, physical systems with just a few elements that can be well-described by formal mathematical models, biological systems display highly non-trivial structures that manifest complexity at multiple scales [2, 3]. Understanding the nature and structure of organized complexity is a canonical problem in modern biology, which considers interactions between ensembles of biomolecules, cells, organs, and individuals. Additionally, beyond mere complexity, biological systems have a clear capacity to

* Co-first author

† tfvarley@uvm.edu

engage in sophisticated self-assembly and repair of complex anatomical structures. This is not merely emergent complexity for its own sake, but rather dynamic problem-solving capacity [3, 4]. Collectives of cells and tissues homeostatically navigate the space of anatomical states during embryogenesis, regeneration, and cancer suppression [5, 6]. These states occur at scales much larger than the cells and molecular networks that implement them, requiring global coordination and virtual governor dynamics that adaptively manipulate subsystems to reach the correct species-specific target morphology and physiological states despite a range of unpredictable circumstances [5, 7]. While biologists intuitively recognize the presence of this high-level organization and control, and have noted its importance for applications in biomedicine [8, 9] and bioengineering [10], quantifying it for rigorous study has proven difficult, due to the inherent difficulties in understanding high-dimensional, multi-scale processes [11]. Parallels between the functionality of electrophysiological networks in the brain and in non-brain tissue have been discussed, because of their common evolutionary and developmental origin, and many invariants across neuro-behavioral and morphogenetic problem-solving [12, 13]. Nevertheless, major knowledge gaps exist with respect to what kind of information patterns are being implemented in neural and non-neural tissues.

The challenge, then, is how can we infer the structure these high-dimensional processes given limited, and often noisey, empirical data? One of the most well-developed approaches is studying how information is distributed over the component elements of the system, and the structure of the dependencies that form the "scaffold" of on-going, spontaneous dynamics [14]. These approaches have been most well-developed in the field of computational neuroscience, where large datasets of high-temporal and high-spatial resolution time series are frequently recorded using methodologies like fMRI, EEG, and MEG [15]. From these data, a whole library of tools have been developed that characterize the structure of multivariate interactions and describe them with a variety of formal statistics.

In the context of neuroscience, these techniques have revealed a rich architecture of different kinds of interactions, between neurons, neuronal networks, and whole regions of cortex [16, 17]. Despite these findings, however, many of these techniques have remained sequestered in neuroscience, leaving it unclear to what extent the patterns observed in the brain are "brain-specific", or if these patterns of brain activity reflect larger features of information processing dynamics across biological systems. The answer to this question would be a contribution to the emerging field of Diverse Intelligence research [18–20], which

seeks to understand how cognitive capacities arise and are adaptively implemented in a wide range of material substrates and problem-spaces.

To do this, we compare temporal information dynamics in two, radically diverse systems: resting state fMRI data from human brains, and calcium signaling data recorded from preparations of embryonic *Xenopus* tissue known colloquially as " Xenobots" [21, 22]. The term "Xenobot" is very broad and refers to a number of different of preparations: here we specifically deal with so-called "basal Xenobots", which represent a kind of default configuration, lacking some of the additional features seen in [21, 22]. The latter are autonomously-motile, self-assembling constructs derived from ectoderm (epidermal progenitor) cells from the frog *Xenopus laevis*, which are used in the field of biorobotics as a chassis in which competencies of living materials in novel configurations can be assessed, and for which techniques to induce novel useful behaviors can be developed [23]. Because of their morphogenetic and behavioral properties, their lack of nervous system, their synthetic (ecologically-unique and novel) nature, and their amenability to optical interrogation, they are an interesting model system to compare to the dynamics observed in neural constructs, which have been under long periods of selection for specific functionality in a fixed configuration. While fMRI data and calcium signals from basal Xenobots represent two radically different biological systems, they share important commonalities: both a basal Xenobot and a brain are a "whole" system which can be subdivided into distinct sub-systems, or "parts" (cortical parcels in fMRI data, individual cells in basal Xenobots). From each of these parcels, we can record time series data, and explore how interactions between lower-level elements (parcels, cells) are structured in relation to each-other, and the collective whole.

Here we systematically explore the presence of higher-order interactions in the basal Xenobot cellular structure, and show that those patterns are similar to those found in the dynamics of the adult human brain. Recent prior work on calcium signaling has shown that xenopus epidermal organoid systems (with no autonomous motion behavior) do show signs of non-trivial functional organization [24], however an in-depth, comparative analysis remains an outstanding question. Multicellular patterns of calcium signaling are widespread in biology, and complex patterns (waves, bursts, and oscillations) have been found in diverse systems, including animal epithelial tissue [25, 26], plant tissue [27], and fungal mycelial networks [28]. These coordinated dynamics have been found to be crucial for many dynamical and self-organizing processing in biology; examples include skin development [29], regener-

ation [30], wound healing [31], and cell-type differentiation [32]. While the role of calcium transients in diverse biological processes is well-developed, and the apparent complexity of multi-cellular patterns of calcium activity have been qualitatively described in terms of waves, oscillations, and other large-scale patterns, a rigorous, formal analysis of multivariate information-processing structures in networks of signaling cells has not been done.

The vast majority of these particular statistics were first developed in the context of theoretical neuroscience for application to the analysis of neuroimaging data, and have been found to correlate with various features of cognition, health, and disease. A systematic review of all the measures can be found in the Materials and Methods, but we will briefly describe them and relevant findings in the context of neuroscience. The first, and most fundamental inference is that of signed, functional connectivity networks that form the architecture of the whole system (see Sec. V D). In the brain, consistent functional connectivity networks have been found in all neuroimaging modalities [33, 34], and include a complex distribution of positively and negatively signed dependencies between brain regions, indicating correlated and anti-correlated patterns of activity. These interactions between positive and negative edges are thought to play a key role in the maintenance of non-trivial structure [35–37], and alterations to the distribution of positive and negative edges has been associated with cognitive and clinical differences [38–41]. The networks themselves are organized hierarchically, with edges arranged into a modular, meso-scale structure of communities with high internal co-fluctuation (associated with positively-signed edges) and anticorrelations between communities [17, 42], and changes in this modular structure are associated with behavioral and cognitive differences as well [43–45]. A limitation of all of these analyses is that they are built on *pairwise* models of interaction: in the functional connectivity framework, the fundamental unit is the bivariate edge, and higher-order interactions can only be inferred indirectly by considering patterns of lower-order interactions [46]. To get around this limitation, there has recently been an increase in interest in truly higher-order interactions in complex systems [47], using techniques from information theory to asses polyadic synergies and redundancies directly. Analysis of neural data has found that these higher-order interactions are widespread throughout the human brain [46, 48], and changes in higher-order interactions have been observed in the context of aging [49–51], neurodegeneration [52], autism [53], schizophrenia [54], and sequel to neurosurgery [55]. All of these statistics are summary statistics, which describe some feature of the *average* structure of

the system. To deepen our analysis, we also explored time-resolved metrics. The first was the variance of the instantaneous co-fluctuation, which describes frame-resolved changes in integration-segregation balance over time [56–59], and the second was the integrated information [60], which measures how much more effectively an observer can predict the future of a whole based on a model of it's true joint statistics versus a disintegrated model. Changes in integrated information have been found to be most closely associated with changes to consciousness following anesthesia or brain injury [61, 62]. This literature from neuroscience shows that patterns of collective behavior are not merely statistical "noise" or some kind mathematical shell game, but rather that they reflect meaningful differences in the underlying processes that generate complex cognition and behavior, sometimes with clinical or quality-of-life implications.

A natural question of this line of work, is whether the comparison of calcium signals from basal Xenobots and fMRI time series from humans is a "fair" comparison; these are different organs, different organisms, different scales, and different imaging modalities. We believe that, first, this difference is as much a feature as it is a bug, as it provides an opportunity to test the extent to which these patters, widespread in brain activity, are actually modality-specific or system-specific, and to think about what reasons could prevent applications of information metrics to specific kinds of materials. Second, these two datatypes are not as different as they appear on first blush. The key similarity is that they both describe a "whole" unit, parcellated into component "parts. " In the basal Xenobot, we have coverage of calcium activity from the camera-facing surface of the bot, while in the fMRI, we have coverage from the entire surface of the brain (the cortex). Contrast this with calcium recordings of spiking neurons (e. g. [63]), which typically only sample a small number of neurons from the whole brain. The "whole" is not recorded from in this case, making the structure of part-whole-relationships inaccessible. The data themselves also have similarities that help facilitate comparison: recordings are generally short (on the order of a few hundred frames), the signals are real-valued (unlike spiking neurons), and generally autocorrelated, which means that a common set of information-theoretic estimators and a common null model can be appropriately used in both cases.

In this paper, we are not comparing brains and basal Xenobots directly (e. g. we are not asking "which system has more total correlation"): differences in system sizes, the properties of the recordings, and variable first order dynamics can introduce complex and hard-to-

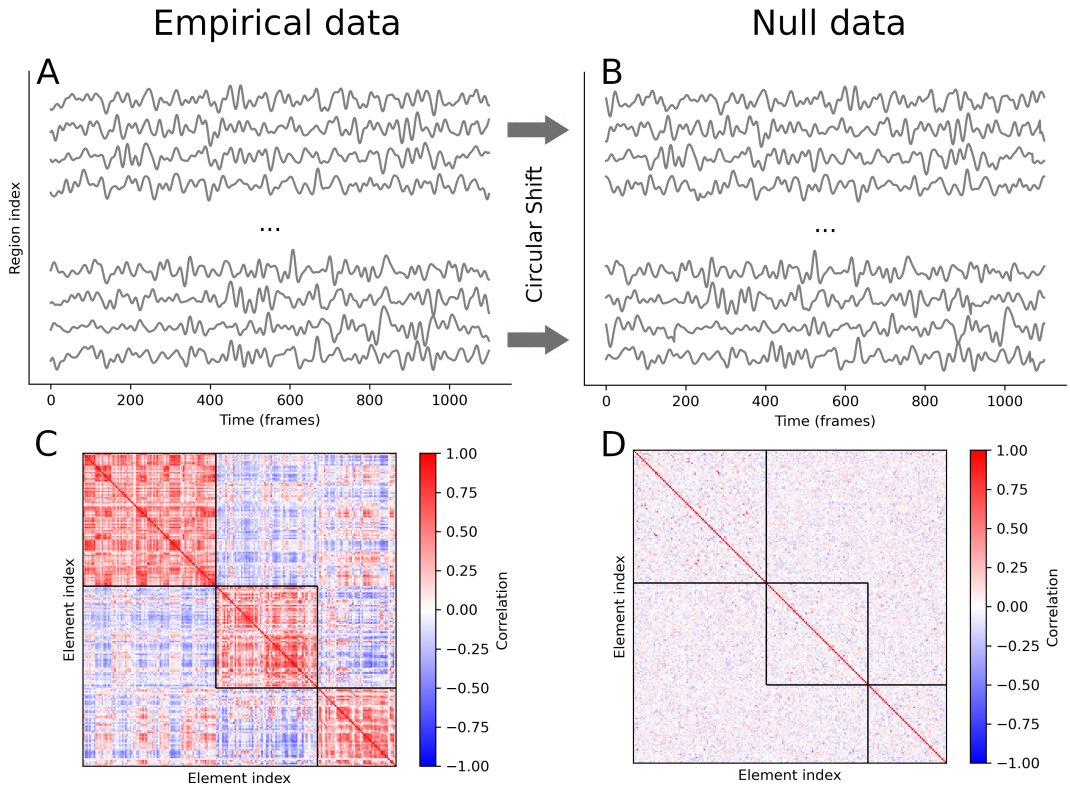

FIG. 1. **The circular shift null model.** **A:** The initial time series data. After applying the circular shift (**B**), the surrogate data preserves all first-order features of the individual elements (autocorrelation, frequency spectrum, etc), although higher-order correlations are disrupted. **C:** the covariance matrix that defines the functional connectivity of the raw data, and **D** is the functional connectivity of the null data (organized into the same community structure in C). It is visually apparent that circular shifting largely disrupts all of the "structure" in the data.

untangle biases in the estimation of information-theoretic quantities [14]. Instead, we show that both systems consistently display greater integration then you would expect if the elements were independent. It is well known that certain lower-order features of a time series can complicate analysis of higher-order interactions [64], requiring careful consideration to avoid Type 1 errors [65]. Doing this requires constructing a bespoke null model for reach fMRI recording and each basal Xenobot that preserves all first-order features of the elements (autocorrelation, frequency spectrum, etc.) while disrupting any interactions between them. To do this, we use a circular-shift null model (for details see Materials and Methods) to preserve first order features while disrupting higher-order interactions between elements.

Morphogenesis is based on coordinated activities of individual cells resulting in a collective outcome. Thus, we hypothesized that, despite being radically different kinds of systems, that

the basal Xenobots would show non-trivial information structure, indicative of complex, higher-order organization, despite the comparative "simplicity" of the system (relative to the brain). Our results largely bear this hypothesis out: we found that, for all measures tested, both the basal Xenobots and the brains showed significantly greater higher-order integration than would be expected in the null case of independent elements with preserved first-order statistics.

II. RESULTS

A. Basal Xenobots show non-trivial, spatially-embedded functional connectivity networks.

In order to determine whether basal Xenobots showed patterns of information integration and emergent dynamics in a manner similar to the human brain, we computed a battery of measures on both calcium signals recorded from basal Xenobots (N=28) and fMRI BOLD signals recording from resting adult human brains (N=50). We found that, despite their comparatively simple biological structure the basal Xenobots displayed every sign of emergent complexity at significantly greater intensities than was observed in surrogate null data that preserved first-order features. When constructing functional connectivity networks, in every single brain, and every single bot, we found that positive and negative functional correlations were widely present, while in the autocorrelation-preserving nulls, there was almost no correlation to speak of. These correlations form the functional connectivity network: every element in the system (cortical parcels from brains, cells for basal Xenobots) forms a vertex, and the weight of the edge between them is the Pearson correlation between their respective time series. When considering the spatial embedding of edges, we found that basal Xenobots displayed a stereotyped pattern also typically found in the brain: a negative correlation relating the Euclidean distance between two cells and the edge dependency between them. All twenty eight bots had statistically significant negative correlations between signed functional edge weight and distance (average $r = -0.124 \pm 0.06$, all p-values less than 10^{-6}). The same pattern was observed in the fMRI data: all brains showed a negative correlation between functional edge weight and Euclidean distance (average $r = -0.237 \pm 0.03$, all p-values less than 10^{-100}). While the distance/functional connectivity relationship was

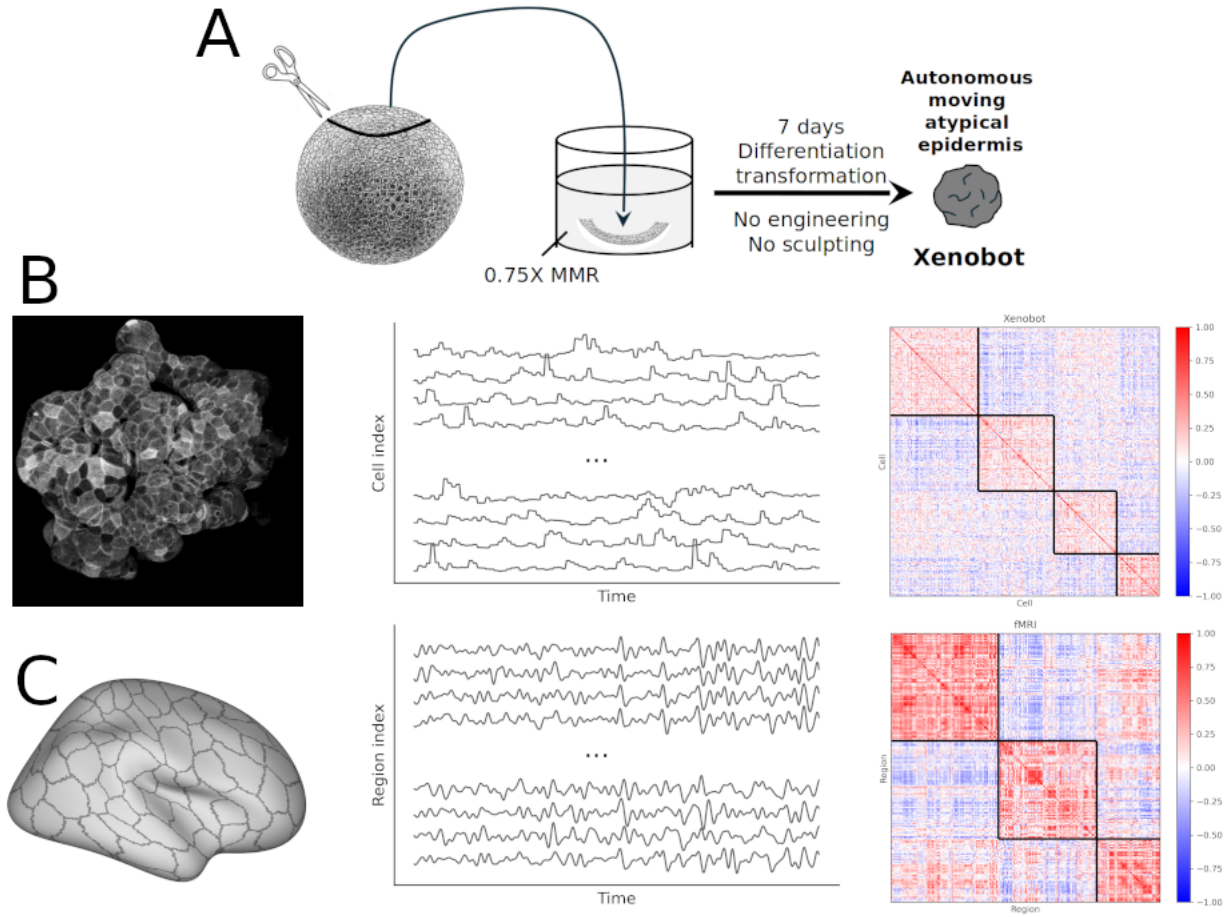

FIG. 2. **Data preparation and matrix construction. A:** This cartoon describes the production of basal Xenobots from frog embryonic tissue. Caps are excised by hand and cultured for seven days without perturbation; the resulting autonomously moving epidermal cell structure is a "basal" (i. e. unmodified) Xenobot. **B:** The pipeline for learning functional connectivity patterns from basal Xenobots. Videos of the bots are segmented into individual cells, from which average calcium traces are extracted. The covariance matrix defines the functional connectivity, which can be organized into meso-scale communities following clustering. **C:** The same pipeline, but for human brain data recorded with an fMRI; in this case, the elements are cortical regions (corresponding to the Schaefer 200 parcellation [66]) and the signal is BOLD rather than calcium, but the overall pipeline remains the same.

certainly weaker in the basal Xenobots than in the brains, we should note that the brain regions are represented in three-dimensional space, while the basal Xenobot cells are only represented in two-dimensional space, reducing the available degrees of freedom. This shows that basal Xenobots have a non-trivial functional structure, more closely resembling the brain than a disintegrated system of independent cells, and that the spatial embedding of bots informs on the kinds of communication that cells can engage in, in a way that is reminiscent of cortical communication. These results also replicate findings first observed in

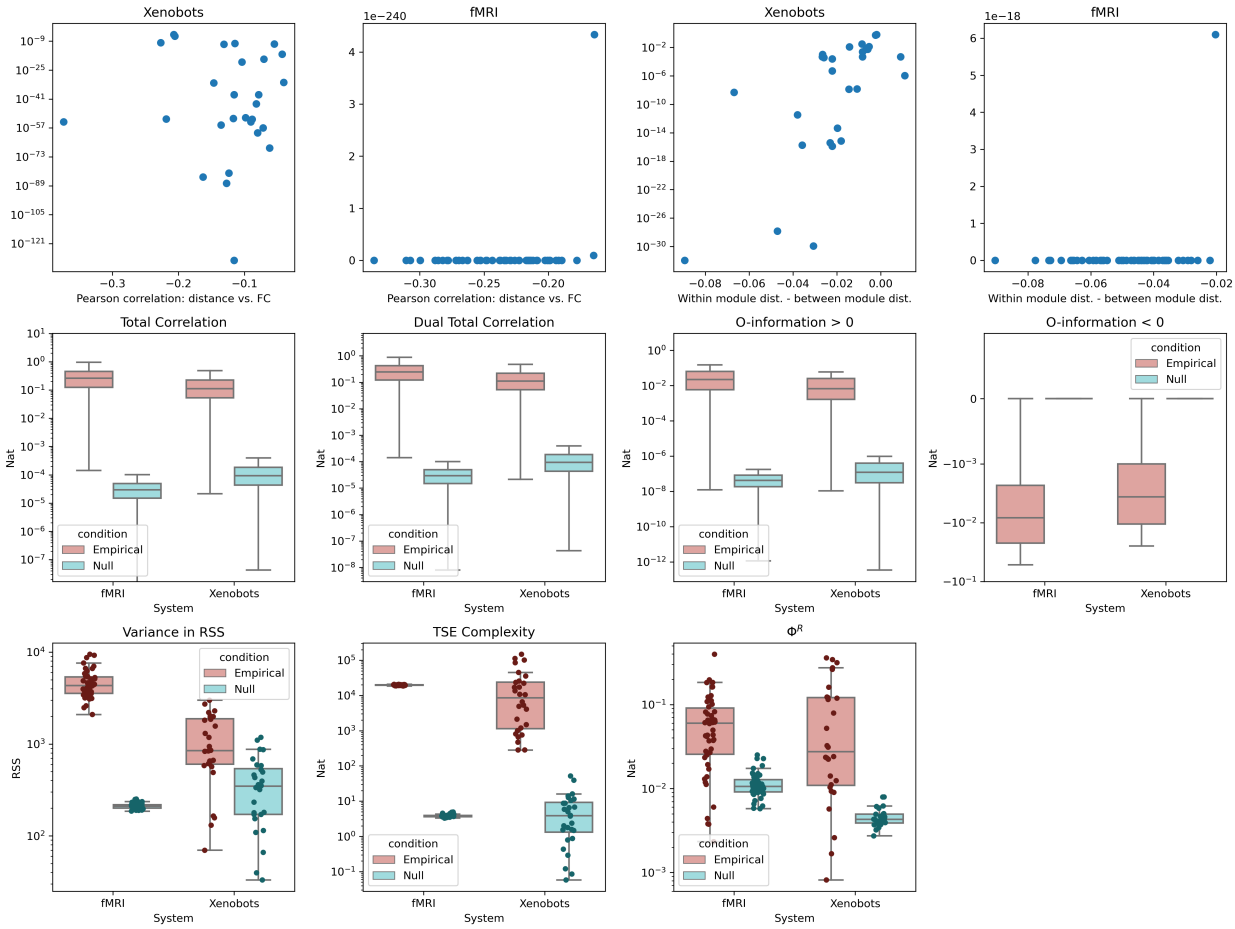

FIG. 3. **Similar expression of complex functional connectiivty structures in basal Xenobots and brains.** **A-B** Scatterplots of the Pearson correlation coefficient of functional connectivity edge strength against Euclidean distance, plotted against the p-value of the correlation. Clearly in both brains and basal Xenobots, there is a strong negative correlation between functional connectivity strength and spatial distance, as would be expected from an embeded system. **C-D**: Scatterplots of the difference between Euclidean distance within functional connectivity modules against the p-value of the difference. There is a consistent pattern that cells within functional modules are also closer to each-other in space. **E-H**: Box plots showing the higher-order structures in sets of three, four, and five elements for total correlation (E), dual total correlation (F), those multiplets with positive O-information (G, indicating redundancy), and those multiplets with negative O-information (H, indicating synergy). **I** The variance in RSS timeseries for each system, compared to the respective nulls. **J** The TSE-complexity for each system, compared to their respective nulls. **K** The corrected whole-minus-sum integrated information Φ^R for each system and their respective nulls.

[24], in a closely-related organoid model system. Multi-resolution community detection [67] finds that, in both brains and bots, these positive and negative correlations are arranged into a meso-scale structure of multiple distinct communities that are internally positively correlated, with anticorrelations between them. These communities group vertices (cortical

parcels in brains, cells in basal Xenobots) into sub-systems that are more strongly connected *within* themselves than they are *between* other groups of vertices. For visualization of example modular covarince matrices, see Figure 2. If we consider the spatial embedding modules, we find that in basal Xenobots, cells that are grouped within modules tend to be closer in space than cells grouped into different modules (average $\Delta = -0.02 \pm 0.02$), with 20 of 28 bots showing a statistically significant difference ($p < 0.05$, Bonferonni corrected). For visualization, see Figure 3C-D. The relationship between spatial embedding and modules was more consistent in the fMRI scans, but followed the same pattern: average $\Delta = -0.047 \pm 0.02$, and all fifty recordings showed a statistically significant difference ($p < 0.05$, Bonferonni corrected). In the brain these modules are associated with distinct functional systems, such as the default mode network, or the fronto-parietal control network [42], but their significance in the bots is decidedly less clear. They may reflect distinct types of cells, or areas that (if normal development were allowed to continue) are destined to differentiate into distinct mature systems. For visualization, see Figure 2A-B.

B. Time-resolved analysis shows dynamic integration and segregation balance

The functional connectivty results describe the *average* dependency between two elements. To assess whether the patterns of co-fluctuation were similar at the highest possible level of temporal resolution, we used an edge time series analysis [56, 68], which decomposes the average correlation into a series of instantaneous couplings (see Materials and Methods). To construct a summary statistic from the edge time series, we considered the variance of the root-sum-squares (RSS) for every frame across every node. The variance of the RSS acts like a crude Fano factor [69]: if all elements are independent, the variance of the RSS will be zero, likewise if all time series are copies of each-other. Variance of RSS is highest when the system combines moments of instantaneous integration and segregation at different times. Both the basal Xenobots and the fMRI scans had a significantly higher empirical variance in the RSS of co-fluctuations than their respective nulls. For visualization, see Figure 3I. The variance for the basal Xenobots was 1168.179 ± 823.86, significantly greater than the basal Xenobot nulls, which had variance of 405.06 ± 308.59 (Cohen's D = 1.227, $p < 10^{-}9$). In the fMRI scans, the variance was 4667.169 ± 1630.249, which was significantly greater than the null variance: 211.797 ± 14.641 (Cohen's D = 3.865, $p < 10^{-}14$). These results

suggest that both the brains and the basal Xenobots have a rich temporal dynamic combining a mixture of transient integration and segregation: in some frames all the cells are co-fluctuating together, while in others they are behaving as if they are independent.

C. Basal Xenobots show emergent, higher-order information dependencies

When considering polyadic information describing coordinated activity between multiple elements, we found that all forms of higher-order information were significantly enriched in both brains and basal Xenobots compared to their respective nulls. So far, all of the measures discussed have been pairwise: describing some feature of the interaction between dyads of elements. To explore genuine higher-order interactions comprising sets of three or more elements, we turned to multiviariate information, and specifically, generalizations of the mutual information: the total correlation, the dual total correlation, and the O-information [70, 71]. The total correlation and dual total correlation both quantity different notions of what it means for a set of multiple variables to "share" information [72, 73], while the O-information gives a heuristic measure of whether the overall information structure is dominated by *redundant* or *synergistic* dependencies [71]. For visualization, see Figure 3E-H. In fMRI scans, across multiplets of size three regions, four regions, and five regions, the average total correlation [72] was 0.326 ± 0.267 nats, significantly greater than their respective nulls $3.5 \times 10^{-5} \pm 2.65 \times 10^{-5}$ nats (Cohen's D $= 1.726$, $p < 10^{-100}$. The same was true with basal Xenobots, which had an average total correlation of 0.2 ± 0.27 nat, greater than the to a null average of 0.00017 ± 0.0003 nat (Cohen's D $= 1.029$, $p < 10^{-100}$). The total correlation can be understood as a measure of functional synchrony, as it is maximal when all time series are copies of each-other, these results suggest that the brains and the basal Xenobots both share features of multi-element synchrony in BOLD and calcium data respectively. The same pattern was true when using the dual total correlation [73]. In fMRI scans, the average dual total correlation was 0.2996 ± 0.228 nat, significantly greater than the null $3.53 \times 10^{-5} \pm 2.65 \times 10^{-5}$ nat (Cohen's D $= 1.859$, $p < 10^{-100}$). Similarly, with basal Xenobots, the empirical average dual total correlation was 0.18 ± 0.22 nat, significantly greater than the null 0.0002 ± 0.0003 nat (Cohen's D $= 1.15$, $p < 10^{-100}$. The dual total correlation quantifies the amount of "entangled information"; information that is duplicated over multiple elements. The finding that both brains and basal Xenobots have significant amounts of dual total

correlation indicates the presence of complex, multivariate interactions binding together information across multiple elements in both systems. When considering the O-information, the analysis is a little more complex, as the sign of the O-information is meaningful in addition to its absolute value: if the sign is negative, then the system in question is dominated by *synergistic* dependencies (information in the whole that is not present in the parts), while if the sign is positive, the system is dominated by *redundant* dependencies (information copied over multiple elements) [71]. Crucially, if the system is comprised of solely bivariate dependencies, then the O-information zero, and by implication, whatever information is visible must be truly polyadic. The simplest analysis is to consider the relative absolute values of the O-information between empirical and null datasets, as that will give a heuristic measure of the presence of beyond-pairwise information (redundant or synergistic). We found that both brains and basal Xenobots had significant polyadic information. In empirical fMRI, the average absolute value of the O-information was 0.039 ± 0.065 nat, significantly greater than the null fMRI data $8.41 \times^{-8} \pm 7.9 \times 10^{-8}$ nats (Cohen's D = 0.852, $p < 10^{-100}$. Similarly, in empirical basal Xenobots, the absolute value of the O-information was 0.016 ± 0.08 nat, significantly greater than the disintegrated null: $9.07 \times 10^{-9} \pm 2.5 \times 10^{-6}$ (Cohen's D = 0.3, $p < 10^{-100}$). Since the O-information can disambiguate between two flavors of higher-order information, we can also break the dataset down into two parts based on sign, representing those multiplets that are redundancy dominated and those multiplets that are synergy-dominated. When we consider only redundancy-dominated multiplets, we find the same pattern as the absolute value of the O-information. The fMRI data had significantly more redundancy (0.05 ± 0.076 nat) than the null data ($6.4e-08 \pm 7.63e-08$, Cohen's D = 0.945, $p < 10^{-100}$, and likewise the basal Xenobots have significantly more redundancy as well (0.036 ± 0.09 nats) than the nulls ($6.35 \times 10^{-7} \pm 2.47\times^{-6}$, Cohen's D = 0.52, $p < 10^{-100}$). When considering the synergy, we find the same pattern: when considering only multiplets with negative O-information, the fMRI data had significantly more synergy (-0.018 ± 0.026 nat) compared to the associated nulls ($-9.16 \times 10^{-8} \pm 7.87 \times 10^{-8}$, Cohen's D = -0.964, $p < 10^{-100}$). The basal Xenobots showed the same pattern, with the empirical data having significantly greater synergy (-0.01 ± 0.023 nat) compared to the associated nulls ($-6.27 \times 10^{-7} \pm 2.36 \times 10^{-6}$, Cohen's D = -0.66, $p < 10^{-100}$). These results show that, not only do basal Xenobots have statistically significant higher-order information, that they have both higher-order redundancies and synergies, in a manner that is typical

of the human brain (as recorded with fMRI). Redundancies and synergies have been found throughout the natural world; beyond brains, synergistic dependencies have also been found in sociological [74] data, climate data [75, 76], economic data [77], psychometric data [78], physical phase changes [79], and even the structure of musical scores [80]. Consequently, higher-order synergy may refelct a very general kind of "integrated sophistication" common to many complex systems.

The final higher-order functional connectivity measure that we used was the Tononi-Sporns-Edelman (TSE) complexity [81], which provides a measure of the balance between integration and segregation (somewhat analogous to the O-information's balance of redundancy and synergy). A high TSE complexity suggests that integration and segregation are co-existing in some non-trivial way. In the fMRI data, we found that the TSE complexity was much greater in the empirical data (19662.089 ± 519.661 nat) compared to the associated nulls (3.82 ± 0.339, Cohen's D $= 53.498$, $p < 10^{1}.7764 \times 10^{-15}$). The same pattern is apparent in the basal Xenobots, with the empirical bots having a very high TSE complexity (24857.58 ± 38739.62) compared to the associated nulls (7.79 ± 11.73, Cohen's D $=$ 0.9, $p < 10^{-9}$). These results collectively show that the functional structure of the basal Xenobots show sophisticated, multi-cell coordination that is highly similar to what is seen in human brain activity. For visualization, see Figure 3J.

D. Basal Xenobots integrate information over time

So far, all of the measures that we have computed are *functional* measures: they model the dynamics of the BOLD signal or calcium signal as independent frames. We also wanted to consider the *effective* connectivity, which quantifies the extent to which the past state of elements discloses information about their collective future: this is a dynamic measure that accounts for the temporal integration of the whole system. To do this we computed the whole-minus-sum integrated information [60, 82], which provides a measure of how much more predictive power there is when modeling the system based on it's true joint statistics compared to the sum of all the parts modeled independently. We computed a corrected version of the integrated information to ensure that it was non-negative [83], for details see Sec V H. We found that both the basal Xenobots and the brain had signfiicantly greater dynamic integrated information compared to their respective nulls. In the fMRI data, the

average integrated information was 0.072 ± 0.071 nat, significantly higher than the associated null 0.012 ± 0.004 (Cohen's D = 1.197, $p < 10^{-11}$). In the basal Xenobots, the average integrated information was 0.09 ± 0.11 nat, significantly greater than the null 0.005 ± 0.001 nat (Cohen's D = 1.072, $p < 10^{-7}$). For visualization, see Figure 3K.

All of these results have fit a common pattern: whatever the measure of structure applied, both the brains and basal Xenobots show statistically significantly greater structure than a null model that preserves lower-order dynamics but disrupts higher-order ones. This suggests that there is a large number of "features" of structural organization that are shared by both basal Xenobots and brains, despite their radically different biological substrates.

III. DISCUSSION

In this paper we have compared two radically different biological systems: adult human brains (as imaged with fMRI [84]) and preparations of embryonic frog tissue colloquially named "basal Xenobots" (expressing a fluorescent calcium reporter). This project was motivated by the recent discovery that related organoids built from embryonic frog tissue display organizational features typically studied in computational neuroscience: functional connectivity networks, high-amplitude co-fluctuations, and response to perturbation [24]. In neuroscience, many of these features of organization are known to associated with meaningful differences in cognitive or clinical states (such as anesthesia, aging, and neurodegeneration), and so the question of how to interpret their presence in non-neural systems is a standing question. We hypothesized that these signs of similarity reflected a deeper, underlying commonality between brains and basal Xenobots, which could be probed with techniques from complex systems science, network science, and multivariate information theory. Moreover, morphogenetic systems, whether natural embryos or synthetic constructs, are distinguished by coherent, coordinated actions of individual cells toward specific outcomes, often featuring the ability to attain the target morphology despite noise or even drastic interventions. Like neurons in a brain which implement an integrated "animal" with competencies, preferences, and memories that belong to it and not to any of its parts, biochemical and bioelectrical networks among cells likewise serve a binding function [85, 86]. They enable cellular collectives to traverse the space of anatomical possibilities as a coherent unit, with all cells cooperating to achieve a large-scale outcome (e.g., the right number of fingers in a regenerating axolotl

limb) that is not defined at the level of a single cell. Thus, we sought to use established methods from neuroscience to attempt to quantify the ability of non-neural cells to process information in a way that reveals a whole distinct from a collection of parts.

We found that, across a battery of measures of statistical organization, including networks, higher-order interactions, dynamic information integration, and time-resolved fluctuation analysis that basal Xenobots display "brain-like" patterns of information, and are universally more organized than a null model that preserves cell-level dynamics. As we will discuss below, these findings raise questions about how to think about modeling both neural and non-neural complex biological systems, and challenge how we interpret many of the statistics that have formed a core part of modern computational neuroscience.

The use of "brain-like" may seem provocative. There are, of course, a tremendous number of ways that basal Xenobots are nothing like human brains: they are different scales, cultured from different physiological systems so the cell types are completely different, and the behaviors each system can display are profoundly different as well. Despite these differences, however, we argue that the claim of brain-likeness remains insightful: almost all of the features explored here have been found to correlate with clinically or cognitively meaningful differences in mental state or behavior. The finding that they are also present in basal Xenobots raises complex philosophical and scientific questions about the nature and purpose of these patterns in Nature. All of these statistics were developed to reveal different kind of "complex" structure: organizational architectures involving the integrated interaction of many different components, largely independent of the specific nature of the individual elements [14]. This is what has motivated the applications in neuroscience, but in theory the notions of information-sharing and dependency revealed by these measures should apply to any system. If we propose that, in brains, these patterns are reflective of fundamental features of the brain's central function, then we have to ask: what are they doing in basal Xenobots? Have we underestimated the information processing capacity of non-neural tissue? Is it possible that the fundamental machinery of cognition is more widespread than it appears and can be instantiated in non-neural tissue, devoid of spikes, neurotransmitters, and the usual biological "wetware" we assume is required for coherent behavior? Conversely, one could argue that the presence of these patterns in (commonly-assumed) non-cognitive, non-conscious embryonic tissue suggests that the neuroscientists exploring these patterns in brains have been chasing statistical epiphenomena; that collec-

tive information, meso-scale modularity, and integration/segregation balance do not actually reveal anything uniquely specific to the brain at all. If this is the case, it would behoove neuroscience as a field (particularly theoretical and computational neuroscience that relies on gross-scale neuroimaging) to reflect on what it is that is being measured, and why. We have no answer to these questions at present. To tackle them will require considerably more detailed analysis of information dynamics in non-neural tissue, as well as more formal and rigorous definitions of what "cognition" or "cognitive processes" might look like in biological systems vastly different from the usual animal models used in neuroscience and cognitive science. The latter is the province of the emerging field of diverse intelligence [19, 20, 87].

The emergence of complex, non-trivial forms of statistical integration has been documented in many models of the brain as a complex system, however, these models almost universally assume that the dynamics are being run on a physical substrate of white-matter connections (e. g. see [88, 89] , which used a Kuramoto model on structural graphs derived from MRI scans of white-matter tracts to explore the relationship between structural topology and functional dynamics). A question for future researchers is to what extent the basal Xenobots show a similar structural network, and whether the patterns of functional connections track the patterns of structural connections in ways similar to what is observed in the brain. It is known that collections of cells can have structural, as well as functional connections: tunneling nanotubes can connect distinct cells [90–92], and can be and reach lengths as long as multiple cell diameters [93], facilitating everything from electrical connectivity to organelle transfer. Unlike white matter connections in the brain, which are reasonably static on short to medium timescales (such as the duration of an fMRI scan), tunneling nanotubes are fragile and dynamic, and also much harder to image, making a "structure/function" analysis currently impossible. Other methods of physical cell-to-cell communication might include exosomes: vesicles containing signaling molecules that are secreted by cells into the extra-cellular space for take-up by (potentially) distant neighbors [94]. Unlike nanotubes, which form one-dimensional links between source cells and target cells, exosomes can diffuse, potentially reaching many cells simultaneously and thereby facilitating one-to-many, or broadcaster, styles of communication that may be better modeled with directed hypergraphs or other higher-order generalizations of the classic functional connectivity network [46].

Beyond the philosophical questions posed by the questions of "brain-likeness", there is then also a practical question: how do the cells engage in this kind of multi-agent coor-

dination? How do redundant and synergistic information emerge between cells? These questions are also key questions in modern neuroscience, and while answers have begun to crystallize, they tend to leverage the network of structural connections that scaffolds the cortex [61, 89, 95], which as noted above, doesn't exist in the basal Xenobots (or any other non-neural tissue, for that matter). Answering these questions, then, will require a more general theory of how systems self-organize and integrate information, one less committed to a particular configuration of biological hardware.

Finally, this work sets the stage for future work on how perturbations can impact the structure of emergent coordination in non-neural tissue. A key conceptual driver of this work is the repeated finding that, in the brain, perturbations and state differences, such as anaethesia, brain injury, aging, neurodivergent developmental differences, and more are reflected in changes to functional connectivity structures [50, 52, 61, 62]. We expect that the same thing will be true in basal and modified Xenobots: that different perturbations or chemical environments will give rise to distinct patterns of global cell-cell coordination. Possible interventions to explore might include anaesthetics, inflammatory signaling molecules such as cytokines, purinergic singaling molecules such as ATP and ADP, or mechanical perturbation (as was done in [24]). Currently, the results of this paper show that these patterns exist, but shed little light on exactly what they mean or how to interpret them: follow-up work detailing how they change will go a long way to making it clear what it is we are observing here.

IV. CONCLUSIONS

Here, we showed that two radically different biological systems: human brains, and basal Xenobots (self-assembling epithelial cell constructs) display a common set of organizational features and dynamics, including sophisticated functional connectivity networks, higher-order information of multiple types, and dynamic integration of information. In human brains, these features have been associated with meaningful differences in cognitive and behavioral state, raising questions about how to interpret their presence in the context of non-neural tissue. Given the lack of (apparent) structural connectivity (a key difference from brains), basal Xenobots displaying complex, emergent statistical structures may have alternative ways of propagating signals and processing them. We propose that these results

show that "brain-like" patterns of information processing may not be specific to the brain at all; that ideas like "information processing" and "information integration", may be even more relevant to non-neural, biological systems than is generally appreciated and the functional similarities between different types of embodied autonomous agents can now be quantified.

V. MATERIALS AND METHODS

A. Xenobot preparation

All experiments were approved by the Tufts University Institutional Animal Care and Use Committee (IACUC) under protocol number M2023-18. Xenopus Laevis embryos were fertilized in vitro according to standard protocols (Sive, 2000) and reared in 0.1X Marc's Modified Ringer's solution and were housed at 14oC and staged according to Nieuwkoop and Faber (Nieuwkoop and Faber, 1994). Embryos were injected with GCamp6s calcium indicator (1-2 ngs per injected blastomere) and lifeAct-mCherry cell membrane and cytoskeletal indicator (0.2-0.5 ngs per injected blastomere) mRNA in both blastomeres at 2-cell stage for uniform expression throughout the embryo. mCherry-Lifeact-7 plasmid was a gift from Michael Davidson (Addgene plasmid # 54491, `http://n2t.net/addgene:54491`, Accessed on 12 August 2022, RRID:Addgene_54491). The most basic version of Xenobots (no sculpting or mixing of different tissues) were generated as described previously. Briefly, stage 9 fertilized injected embryos were placed in a petri dish coated with 1% agarose made in 0.75X MMR and containing 0.75X MMR solution. Vitelline membrane was removed from the embryos using surgical forceps followed by cutting of the animal cap epidermal progenitor cells. The animal cap explants were placed on the agarose with inside surface facing up. The explants round up into spherical tissue over two hours. These explants were provided fresh dish and 0.75X MMR solution daily. Over 7 days the explant tissue differentiates and transforms into an autonomously moving synthetic epidermal entity aka Xenobot. The day 7 mature autonomously moving Xenobots were used for calcium imaging.

B. Calcium imaging and video processing

Xenobots were imaged using Leica Stellaris Sp8 confocal microscope. Each Xenobot was imaged for 15 mins with a capture rate of one Z-stack projection every 10 secs. GCamp6s and

LifeAct-mCherry were imaged in parallel with separate excitation wavelengths and separate detectors.

Individual cells in the videos were identified and segmented using Cellpose, a generalized deep learning algorithm [96]. Segmentation was performed on a representative image constructed by averaging the frames in the video converted to grayscale. As there was little movement between frames, this was sufficient to provide a good representation of the cell boundaries over the course of the video. The resulting cell segmentations were overlayed on the frames from the green fluorescence channel, which captured GCaMP6s expression, and the average pixel intensity within each cell boundary was extracted to produce a time series of calcium signal intensities localized to individual cells over the duration of the videos. Code for video preprocessing can be found at `https://github.com/caitlingrasso/calcium-signal-extraction`.

Finally, the multivariate calcium traces underwent global signal regression to remove image-wide features

C. fMRI acquisition and pre-processing

These data have been previously published on [46, 48, 88], and so we will present a minimal discussion here and refer to earlier references for the full details of the pre-processing pipeline. The data were taken from the Humman Connectome Project dataset [97]. All participants provided informed consent, and the Washington University IRB approved all protocols and procedures. A Siemens 3T Connectom Skyra equipped with a 32-channel head coil was used to collect data. Resting-state functional MRI data was acquired during four scans on two separate days. This was done with a gradient-echo echo-planar imaging (EPI) sequence (scan duration: 14:33 min; eyes open). Acquisition parameters of TR = 720 ms, TE = 33.1 ms, 52° flip angle, isotropic voxel resolution = 2 mm, with a multiband factor of 8 were used for data collection. A parcellation scheme covering the cerebral cortex developed in [66] was used to map functional data to 200 regions.

Of the 100 unrelated subjects considered in the original dataset, 50 were retained for inclusion in empirical analysis in this study. Exclusion criteria were established before the present study was conducted. They included the mean and mean absolute deviation of the relative root mean square (RMS) motion across either four resting-state MRI scans or one

diffusion MRI scan, resulting in four summary motion measures. Subjects that exceeded 1.5 times the interquartile range (in the adverse direction) of the measurement distribution in two or more of these measures were excluded.

D. Functional connectivity network inference

To build bivariate network models of the brains and the basal Xenobots, we followed a standard functional connectivity inference pipeline [16]. For every pair of elements X_i, X_j, we computed the Pearson correlation coefficient between their associated z-scored timeseries, which defines an $N \times N$ matrix $\mathbf{W}$ that can be interpreted as the adjacency matrix of a weighted, undirected graph $\mathbf{G}$. We opted not to threshold the resulting covariance matrices for several reasons. The first is to maintain the link between functional connectivity matrices and Gaussian probability distributions leveraged by the higher-order information analysis, and the second was to avoid adding biases to the networks that can result from *ad hoc* thresholding procedures [84, 98, 99].

To construct a null network, we took a circular-shifting approach: each individual time-series was randomly shifted to the left or right, independently of each other, to construct a surrogate dataset that preserved all first-order features of each signal (autocorrelation, frequency spectrum, etc), but disrupted all coupling between them. A null functional connectivity network was then constructed, and averaged, over 1000 such instances, to create a single null "twin" for each basal Xenobot and fMRI recording. This null network contains all *apparent* higher-order information that is actually attributable to lower-order features such as autocorrelation, with the *true* higher-order information being erased.

E. Community detection

To explore the meso-scale network structure of brains and basal Xenobots, we clustered the signed functional connectivity networks, following standard pipelines in computational neuroscience [42]. For a graph $\mathbf{G} = \{\mathbf{V}, \mathbf{W}\}$, where $\mathbf{V}$ is the vertex set and $\mathbf{W}$ is the adjacency matrix of weighted edges, the standard approach to community detection involves finding the partition σ of the system $\mathbf{G}$ that maximizes the modularity quality function. We used the Leiden algorithm with a constant Potts model [100] to optimize the quality function:

$$Q(\mathbf{G}, \sigma, \gamma) = \sum_{V_i, V_j \in \mathbf{V}} (\mathbf{W}_{ij} - \gamma)\delta(\sigma_i, \sigma_j) \tag{1}$$

where $\mathbf{W}_{ij}$ is weight of the edge connecting vertices V_i and V_j in the graph $\mathbf{G}$, and $\delta(\sigma_i, \sigma_j)$ is a delta function that returns 1 if V_i and V_j are in the same partition, and 0 otherwise. Finally, γ is a constant resolution parameter that determines whether the modularity function is biased towards large communities or small ones [101]. While many papers present the modularity as an intrinsic feature of a network, like the average degree, or clustering coefficinet, it is important to note that modularity is actually a feature of a partition *on* a graph, and subject to the resolution parameter. As such there is not a single "optimal" modularity or partition, but rather a space of viable partitions that must be summarized in a reasonable way. To this end we took a multi-resolution, consensus-based approach.

Ordinarily, γ is a free parameter that must be set in an *ad hoc* fashion, however here we adapt a modified version of the multiresolution consensus clustering algorithm [67]: we swept the value of γ in the range from the minimum edge weight in $\mathbf{W}$ to the maximum edge weight in $\mathbf{W}$ in 100 steps, optimizing the partition σ each time, and then computed a consensus partition [102] on the distribution of optimal partitions. Finally, this consensus matrix was clustered using the classic Newman-Girvan modularity with $\gamma = 1$ [103]. This returns a map of the optimal community structure of the network that accounts for every meaningful scale. All optimizations were done using the LeidenAlg package in Python [104].

F. Co-fluctuation analysis

The functional connectivity analyses and their higher-order generalizations describe the expected statistical structure of a system over the duration of the entire recording. While the spatial features (e. g. cells, brain regions, etc) are preserved, the dynamic features are collapsed across time into a single summary statistic [105]. To assess whether the time-resolved dynamics between brains and basal Xenobots were similar, in addition to their long-term structures, we considered the patterns of instantaneous pairwise co-fluctuations. For each pair of cells, X_i and X_j, we constructed an "edge timeseries" [56, 68]:

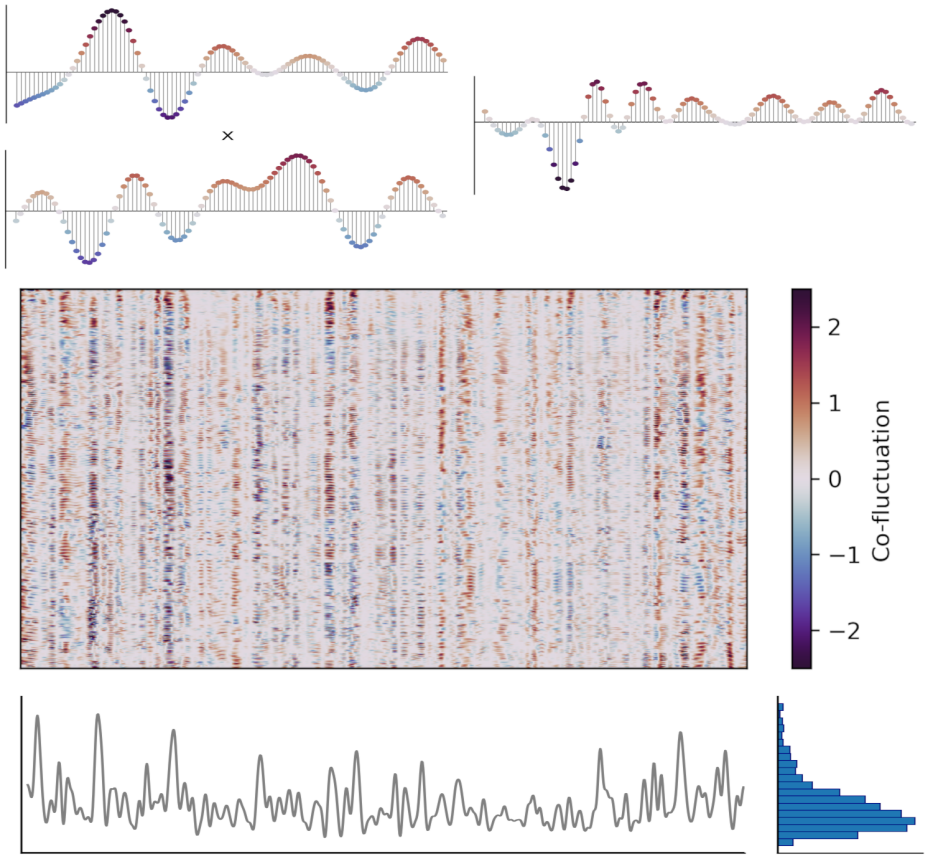

FIG. 4. **Edge connectivity and RSS**.

$$eTS(X_i, X_j) = X_i \odot X_j \tag{2}$$

where $\odot$ is the Hadamard product between the two timeseries. By doing this for all pairs, we construct a new set of of $N^2 - N/2$ edge timeseries, which tracks the instantaneous co-fluctuations of each pair of cells. If, at time t, both cells activity traces are both above or below their means, then the edge timeseries at time t will be positive, while if the cells are fluctuating in opposite directions, the co-fluctuation will be negative.

To construct a time resolved summary statistic of the global edge timeseries, we computed the root-sum-of-squares for each frame [88]:

$$RSS(t) = \sqrt{\sum_{i,j=1}^{N} (X_i^t \odot X_j^t)^2} \tag{3}$$

This produces a univariate timeries that tracks the global magnitude of the co-fluctuations at each moment. We then computed the variance of the RSS timeseries, which acts as a kind of weak Fano factor [69], applied to a variable continuous signal. If every $X_i \perp X_j$, then the variance of the RSS timeseries will be low (as there will be few large co-fluctuations), while if the whole system is totally synchronized, the variance will also be low, as everything is fluctuating together. When the variance is high, there is a dynamic mixture of global integration (high collective co-fluctuation) and segregation (cells are activating independently, with low co-fluctuations).

We used the same circular-shift nulls described above to compute null edge timeseries and null RSS timeseries that preserve all lower-order patterns of activity, but disrupt higher-order coordination.

G. Higher-order information

Most statistical approaches to functional architecture in biological systems have been based on bivariate network models. While powerful, these models are limited by the fact that they can only directly assess interactions between pairs of two regions (e. g. the Pearson correlation or mutual information). Interactions between sets of three or more variables can only be inferred obliquely, as they must be constructed out of lower-order, bivariate relationships. To address this limitation, we also explore higher-order interactions between elements directly using several multivariate extensions of the classic Shannon mutual information. The first is the total correlation [72]:

$$TC(\mathbf{X}) := \sum_{i=1}^{N} H(X_i) - H(\mathbf{X}). \tag{4}$$

Where $H()$ is the Shannon entropy function. The total correlation is a measure of how strongly a given system $\mathbf{X}$ deviates from the null case of total independence among all it's

constituent elements. It is zero if ever $X_i \perp X_j$, and it is maximal if every X_i is a deterministic function of some other X_j (for example, if all elements are perfectly synchronized). The second measure is the dual total correlation [72]:

$$DTC(\mathbf{X}) := H(\mathbf{X}) - \sum_{i=1}^{N} H(X_i|\mathbf{X}^{-i}) \tag{5}$$

where $\mathbf{X}^{-i}$ refers to the joint state of every element of $\mathbf{X}$ *excluding* X_i. Interestingly, the dual total correlation is low both when all the elements are independent, but also when they are all synchronized. It is high in an interstitial region where information is shared between many elements simultaneously, but not redundantly duplicated over all of them. Due to this, it has been referred to as a "genuine" higher-order interaction [52].

The third measure of higher-order interaction we considered is the O-information [71]:

$$\Omega(\mathbf{X}) := TC(\mathbf{X}) - DTC(\mathbf{X}). \tag{6}$$

The O-information is an unusual measure in that its sign can reveal global features of the organization of $\mathbf{X}$. If $\Omega(\mathbf{X}) < 0$, then the structure of $\mathbf{X}$ is dominated by synergistic interactions (i. e. information is present in the joint state of $\mathbf{X}$ and not any subset), while if $\Omega(\mathbf{X}) > 0$, the $\mathbf{X}$ is dominated by redundant interactions. Recently, Varley, Pope et al. [48], derived an alternative formalization of the O-information that clarifies the nature of the measure:

$$\Omega(\mathbf{X}) = (2 - N) \times TC(\mathbf{X}) + \sum_{i=1}^{N} TC(\mathbf{X}^{-i}) \tag{7}$$

which shows that the O-information can be seen as a measure of whether the deviation from independence in $\mathbf{X}$ is better understood as occurring globally, or in some subset of $\mathbf{X}$.

Finally, the last measure that we used was the Tononi-Sporns-Edelman complexity [81], which provides a global measure of integration/segregation balance:

$$TSE(\mathbf{X}) := \sum_{i=2}^{N} \left(\frac{i}{N} TC(\mathbf{X}) - \mathbb{E}\left[TC(\mathbf{X}^{|i|}) \right] \right) \tag{8}$$

where $\mathbb{E}\left[TC(\mathbf{X}^{|i|}) \right]$ refers to the expected total correlation of all subsets of $\mathbf{X}$ of size i. Like the DTC, the TSE is a non-monotonic measure: it is low if $\mathbf{X}$ is totally disintegrated and if $\mathbf{X}$ is totally synchronized, although unlike the DTC, it sweeps all possible scales of the system in sequence. Analytic work has found that the TSE complexity has a nuanced relationship with redundancy and synergy: synergy positively contributes to the complexity, while redundancy is penalized, pointing to a rich link between integration/segregation balance and redundancy/synergy balance [106].

Since computing the full TSE complexity requires brute-forcing every possible bipartition of $\mathbf{X}$, which is impossible for large systems, we took a sub-sampling approach, as in [48, 107]. If the number of subsets of $\mathbf{X}$ of size i was greater than 100, we randomly sampled 100 subsets to estimate the expected value.

We used the same circular-shift nulls generated above in these analyses as well. The null functional connectivity matrices also double as null covariance matrices, and so each randomly sampled subset of brain regions was also compared to that same subset in the associated null covariance matrix.

H. Dynamic integrated information

All of the results that we have discussed here have been static measures of statistical structure, assuming that joint states are drawn at random from some underlying mulitvariate probability distribution. These approaches don't assess the dynamic nature of biological organisms: the past state of an organism informs on the future state in non-trivial ways. The space of possible dynamic measures is vast, however, in keeping with our focus on multivariate information integration, we chose to use the integrated information coefficient [60], which measures the degree to which the future of a system $\mathbf{X}^{t+1}$ is better predicted based on its own statistics, versus a null model that assumes that all $X^i \in \mathbf{X}$ are independent. Formally:

$$\Phi^{WMS}(\mathbf{X}) := I(\mathbf{X}^t; \mathbf{X}^{t+1}) - \sum_{i=1}^{2} I(X_i^t; X_i^{t+1}) \tag{9}$$

where $\mathbf{X}^t$ is the present state of $\mathbf{X}$, $\mathbf{X}^{t+1}$ is the state of $\mathbf{X}$ after one timestep, and WMS refers to the "whole-minus-sum" interpretation given above.

Intuitively, the Φ function can be understood as quantifying the extent to which the "whole" $\mathbf{X}$ is greater than the sum of it's parts. If $\Phi(\mathbf{X}) = 0$, then there is no higher-order information in the joint-state of the whole that is not learnable when considering the parts individually. $\mathbf{X}$ could be modeled just as effectively as a set of disintegrated independent processes as opposed to a coherent "whole. " A peculiar feature of the Φ function is that it can be negative, suggesting that a system is somehow less than the sum of its parts. Interpreting this stood as a long-term challenge for information theorists until Mediano et al. [83] showed that this occurred when X_1 and X_2 are highly correlated: i. e. that there is so much redundancy that it "swamps" the higher-order interaction. To address this, they introduced a correction:

$$\Phi^R(\mathbf{X}) := \Phi^{WMS}(\mathbf{X}) + \min_{i,j} I(X_t^i; X_{t+1}^j) \tag{10}$$

which is guaranteed to be non-negative and captures only those information-sharing modes that engage the whole system.

1. *Estimating the minimum information bipartition*

Since the Φ^{WMS} is only defined for bivariate systems, computing it for the multi-cellular basal Xenobots required finding an appropriate bipartition of the system. Different bipartitions may return different values of Φ^{WMS}, and so it is generally required that the statistic be computed with respect to the minimum information bipartition [60, 108]: that bipartition that minimizes the integrated information. This is a non-trivial optimization problem (equivalent to minimal cut problems in graph theory), and it is generally infeasible to brute-force search all possible cuts. As such, a number of heuristics have been applied over the years. Here we use the Kernighan-Lin bipartition algorithm [109], as implemented in the Networkx package [110]. Following [111], we began with the bivariate effective connectivity graph: for each pair of regions X_i, X_j, we computed the mutual information between $X_i^t; X_j^{t+1}$ to

construct weighted, undirected graph, which was then bipartitioned. The Kernighan-Lin algorithm was selected due to it's computational efficiency and because it produces equally sized bipartitions, ensuring a balanced bisection of the bots.

Finally, we averaged the timeseries of all elements in each half to extract the global signal for each partition. These were the two time series on which we computed Φ^{WMS} and Φ^{R}. As a null model, we computed a distribution of 1000 autocorrelation-preserving nulls using a circular shift randomization, and re-computed the Φ^{WMS} and Φ^{R} statistics to compare the empirical values to.

I. Gaussian information theory

Information theory is typically used for discrete random variables, however, closed-form, analytic estimators of all the quantities used here exist for continuous, Gaussian random variables [**?**]. Here we will briefly introduce the basic definitions. The mutual information between two univariate variables is given by:

$$I(X_1, X_2) = \frac{-\ln(1 - r^2)}{2} \tag{11}$$

where r is the Pearson correlation coefficient between X_1 and X_2. The mutual information between two multivariate random variables is given by:

$$I(\mathbf{X}; \mathbf{Y}) = \frac{1}{2} \ln \frac{|\Sigma_{\mathbf{X}}||\Sigma_{\mathbf{Y}}|}{|\Sigma_{\mathbf{XY}}|} \tag{12}$$

where $|\Sigma_{\mathbf{X}}|$ is the determinant of the covariance matrix of $\mathbf{X}$, and $\Sigma_{\mathbf{XY}}$ is the joint covariance matrix of $\mathbf{X}$ and $\mathbf{Y}$. The total correlation is:

$$TC(\mathbf{X}) = \frac{-\ln|\Sigma_{\mathbf{X}}|}{2}. \tag{13}$$

These identities are sufficient to compute all information-theoretic measures reported herein.

Acknowledgments

This work was supported by the Cold Regions Research and Engineering Laboratory (CRREL) under Contract No. W913E524C0012.

[1] W. Weaver, engScience and complexity, American Scientist **36**, 536 (1948), number: 4.

[2] O. Artime and M. De Domenico, From the origin of life to pandemics: emergent phenomena in complex systems, Philosophical Transactions of the Royal Society A: Mathematical, Physical and Engineering Sciences **380**, 20200410 (2022), publisher: Royal Society.

[3] P. McMillen and M. Levin, enCollective intelligence: A unifying concept for integrating biology across scales and substrates, Communications Biology **7**, 1 (2024), publisher: Nature Publishing Group.

[4] M. Levin, enCollective Intelligence of Morphogenesis as a Teleonomic Process, in en*Evolution "On Purpose": Teleonomy in Living Systems* (The MIT Press, Boston, MA, 2023).

[5] C. Fields and M. Levin, enCompetency in Navigating Arbitrary Spaces as an Invariant for Analyzing Cognition in Diverse Embodiments, Entropy **24**, 819 (2022), number: 6 Publisher: Multidisciplinary Digital Publishing Institute.

[6] M. Levin, engDarwin's agential materials: evolutionary implications of multiscale competency in developmental biology, Cellular and molecular life sciences: CMLS **80**, 142 (2023).

[7] G. Pezzulo and M. Levin, Top-down models in biology: explanation and control of complex living systems above the molecular level, Journal of The Royal Society Interface **13**, 20160555 (2016), publisher: Royal Society.

[8] E. Lagasse and M. Levin, EnglishFuture medicine: from molecular pathways to the collective intelligence of the body, Trends in Molecular Medicine **29**, 687 (2023), publisher: Elsevier.

[9] J. Mathews, A. J. Chang, L. Devlin, and M. Levin, engCellular signaling pathways as plastic, proto-cognitive systems: Implications for biomedicine, Patterns (New York, N.Y.) **4**, 100737 (2023).

[10] J. Davies and M. Levin, enSynthetic morphology with agential materials, Nature Reviews Bioengineering **1**, 46 (2023), publisher: Nature Publishing Group.

[11] E. Hoel and M. Levin, Emergence of informative higher scales in biological systems: a computational toolkit for optimal prediction and control, Communicative & Integrative Biology **13**, 108 (2020).

[12] C. Fields, J. Bischof, and M. Levin, engMorphological Coordination: A Common Ancestral Function Unifying Neural and Non-Neural Signaling, Physiology (Bethesda, Md.) **35**, 16 (2020).

[13] G. Pezzulo and M. Levin, Re-membering the body: applications of computational neuroscience to the top-down control of regeneration of limbs and other complex organs, Integrative Biology **7**, 1487 (2015).

[14] T. F. Varley, Information Theory for Complex Systems Scientists (2024), arXiv:2304.12482 [physics, q-bio, stat].

[15] N. M. Timme and C. Lapish, enA Tutorial for Information Theory in Neuroscience, eNeuro **5**, ENEURO.0052 (2018), number: 3.

[16] O. Sporns, en*Networks of the Brain* (MIT Press, 2010).

[17] A. Fornito, A. Zalesky, and E. Bullmore, en*Fundamentals of Brain Network Analysis* (Elsevier, 2016).

[18] F. Baluška and M. Levin, EnglishOn Having No Head: Cognition throughout Biological Systems, Frontiers in Psychology **7**, 10.3389/fpsyg.2016.00902 (2016), publisher: Frontiers.

[19] P. Lyon, engThe biogenic approach to cognition, Cognitive Processing **7**, 11 (2006).

[20] P. Lyon, EnglishThe cognitive cell: bacterial behavior reconsidered, Frontiers in Microbiology **6**, 10.3389/fmicb.2015.00264 (2015), publisher: Frontiers.

[21] S. Kriegman, D. Blackiston, M. Levin, and J. Bongard, enA scalable pipeline for designing reconfigurable organisms, Proceedings of the National Academy of Sciences of the United States of America **117**, 1853 (2020), publisher: National Academy of Sciences.

[22] S. Kriegman, D. Blackiston, M. Levin, and J. Bongard, Kinematic self-replication in reconfigurable organisms, Proceedings of the National Academy of Sciences of the United States of America **118**, e2112672118 (2021).

[23] D. Blackiston, S. Kriegman, J. Bongard, and M. Levin, Biological Robots: Perspectives on an Emerging Interdisciplinary Field, Soft Robotics **10**, 674 (2023), publisher: Mary Ann Liebert, Inc., publishers.

[24] D. Blackiston, H. Dromiack, C. Grasso, T. F. Varley, D. G. Moore, K. Srinivasan, O. Sporns, J. Bongard, M. Levin, and S. I. Walker, enRevealing non-trivial information structures in aneural biological tissues via functional connectivity (2024), pages: 2024.05.09.593467 Section: New Results.

[25] R. Balaji, C. Bielmeier, H. Harz, J. Bates, C. Stadler, A. Hildebrand, and A.-K. Classen, enCalcium spikes, waves and oscillations in a large, patterned epithelial tissue, Scientific Reports **7**, 42786 (2017), publisher: Nature Publishing Group.

[26] V. Donati, C. Peres, C. Nardin, F. Scavizzi, M. Raspa, C. D. Ciubotaru, M. Bortolozzi, M. G. Pedersen, and F. Mammano, engCalcium Signaling in the Photodamaged Skin: In Vivo Experiments and Mathematical Modeling, Function (Oxford, England) **3**, zqab064 (2022).

[27] W. Tian, C. Wang, Q. Gao, L. Li, and S. Luan, enCalcium spikes, waves and oscillations in plant development and biotic interactions, Nature Plants **6**, 750 (2020), publisher: Nature Publishing Group.

[28] A. Itani, S. Masuo, R. Yamamoto, T. Serizawa, Y. Fukasawa, N. Takaya, M. Toyota, S. Betsuyaku, and N. Takeshita, Local calcium signal transmission in mycelial network exhibits decentralized stress responses, PNAS Nexus **2**, pgad012 (2023).

[29] N. Christodoulou and P. A. Skourides, enCalcium transients regulate epithelial integration of multiciliated cells during Xenopus skin development (2024), pages: 2024.11.01.621480 Section: New Results.

[30] J. L. Moore, D. Bhaskar, F. Gao, C. Matte-Martone, S. Du, E. Lathrop, S. Ganesan, L. Shao, R. Norris, N. Campamà Sanz, K. Annusver, M. Kasper, A. Cox, C. Hendry, B. Rieck, S. Krishnaswamy, and V. Greco, engCell cycle controls long-range calcium signaling in the regenerating epidermis, The Journal of Cell Biology **222**, e202302095 (2023).

[31] T. Subramaniam, M. B. Fauzi, Y. Lokanathan, and J. X. Law, enThe Role of Calcium in Wound Healing, International Journal of Molecular Sciences **22**, 6486 (2021), number: 12 Publisher: Multidisciplinary Digital Publishing Institute.

[32] C. Leclerc, S. E. Webb, C. Daguzan, M. Moreau, and A. L. Miller, engImaging patterns of calcium transients during neural induction in Xenopus laevis embryos, Journal of Cell Science **113 Pt 19**, 3519 (2000).

[33] P. Garcés, E. Pereda, J. A. Hernández-Tamames, F. Del-Pozo, F. Maestú, and J. Ángel Pineda-Pardo, enMultimodal description of whole brain connectivity: A comparison of

resting state MEG, fMRI, and DWI, Human Brain Mapping **37**, 20 (2016), _eprint: https://onlinelibrary.wiley.com/doi/pdf/10.1002/hbm.22995.

[34] J. Wirsich, J. Jorge, G. R. Iannotti, E. A. Shamshiri, F. Grouiller, R. Abreu, F. Lazeyras, A.-L. Giraud, R. Gruetter, S. Sadaghiani, and S. Vulliémoz, The relationship between EEG and fMRI connectomes is reproducible across simultaneous EEG-fMRI studies from 1.5T to 7T, NeuroImage **231**, 117864 (2021).

[35] M. Saberi, R. Khosrowabadi, A. Khatibi, B. Misic, and G. Jafari, enTopological impact of negative links on the stability of resting-state brain network, Scientific Reports **11**, 2176 (2021), publisher: Nature Publishing Group.

[36] M. Saberi, R. Khosrowabadi, A. Khatibi, B. Misic, and G. Jafari, Pattern of frustration formation in the functional brain network, Network Neuroscience **6**, 1334 (2022).

[37] L. Zhan, L. M. Jenkins, O. E. Wolfson, J. J. GadElkarim, K. Nocito, P. M. Thompson, O. A. Ajilore, M. K. Chung, and A. D. Leow, enThe significance of negative correlations in brain connectivity, Journal of Comparative Neurology **525**, 3251 (2017).

[38] F. Soleymani, R. Khosrowabadi, M. M. Pedram, and J. Hatami, enImpact of negative links on the structural balance of brain functional network during emotion processing, Scientific Reports **13**, 15983 (2023), publisher: Nature Publishing Group.

[39] B. Cao, Y. Chen, R. Yu, L. Chen, P. Chen, Y. Weng, Q. Chen, J. Song, Q. Xie, and R. Huang, Abnormal dynamic properties of functional connectivity in disorders of consciousness, NeuroImage: Clinical **24**, 102071 (2019).

[40] A. R. Aruldass, M. G. Kitzbichler, S. E. Morgan, S. Lim, M.-E. Lynall, L. Turner, P. Vertes, J. Cavanagh, P. Cowen, C. M. Pariante, N. A. Harrison, and E. T. Bullmore, Dysconnectivity of a brain functional network was associated with blood inflammatory markers in depression, Brain, Behavior, and Immunity **98**, 299 (2021).

[41] T. Nir, Y. Jacob, K.-H. Huang, A. E. Schwartz, J. W. Brallier, H. Ahn, P. Kundu, C. Y. Tang, B. N. Delman, P. J. McCormick, M. Sano, S. Deiner, M. G. Baxter, and J. S. Mincer, Resting-state functional connectivity in early postanaesthesia recovery is characterised by globally reduced anticorrelations, BJA: British Journal of Anaesthesia **125**, 529 (2020).

[42] R. F. Betzel, enCommunity detection in network neuroscience, arXiv:2011.06723 [q-bio] (2020), arXiv: 2011.06723.

[43] M. R. Brier, J. B. Thomas, A. M. Fagan, J. Hassenstab, D. M. Holtzman, T. L. Benzinger, J. C. Morris, and B. M. Ances, Functional connectivity and graph theory in preclinical Alzheimer's disease, Neurobiology of Aging **35**, 757 (2014).

[44] E. Tagliazucchi, L. Roseman, M. Kaelen, C. Orban, S. D. Muthukumaraswamy, K. Murphy, H. Laufs, R. Leech, J. McGonigle, N. Crossley, E. Bullmore, T. Williams, M. Bolstridge, A. Feilding, D. J. Nutt, and R. Carhart-Harris, EnglishIncreased Global Functional Connectivity Correlates with LSD-Induced Ego Dissolution, Current Biology **26**, 1043 (2016), publisher: Elsevier.

[45] J. Song, R. M. Birn, M. Boly, T. B. Meier, V. A. Nair, M. E. Meyerand, and V. Prabhakaran, Age-Related Reorganizational Changes in Modularity and Functional Connectivity of Human Brain Networks, Brain Connectivity **4**, 662 (2014), publisher: Mary Ann Liebert, Inc., publishers.

[46] T. F. Varley, M. Pope, P. Maria Grazia, F. Joshua, and O. Sporns, Partial entropy decomposition reveals higher-order information structures in human brain activity, Proceedings of the National Academy of Sciences **120**, e2300888120 (2023), publisher: Proceedings of the National Academy of Sciences.

[47] F. E. Rosas, P. A. M. Mediano, A. I. Luppi, T. F. Varley, J. T. Lizier, S. Stramaglia, H. J. Jensen, and D. Marinazzo, enDisentangling high-order mechanisms and high-order behaviours in complex systems, Nature Physics , 1 (2022), publisher: Nature Publishing Group.

[48] T. F. Varley, M. Pope, J. Faskowitz, and O. Sporns, enMultivariate information theory uncovers synergistic subsystems of the human cerebral cortex, Communications Biology **6**, 1 (2023), number: 1 Publisher: Nature Publishing Group.

[49] M. Gatica, R. Cofré, P. A. Mediano, F. E. Rosas, P. Orio, I. Diez, S. P. Swinnen, and J. M. Cortes, High-Order Interdependencies in the Aging Brain, Brain Connectivity 10.1089/brain.2020.0982 (2021), publisher: Mary Ann Liebert, Inc., publishers.

[50] M. Gatica, C. Atkinson-Clement, P. A. M. Mediano, M. Alkhawashki, J. Ross, J. Sallet, and M. Kaiser, Transcranial ultrasound stimulation effect in the redundant and synergistic networks consistent across macaques, Network Neuroscience , 1 (2024).

[51] M. G. Puxeddu, M. Pope, T. F. Varley, J. Faskowitz, and O. Sporns, enLeveraging multivariate information for community detection in functional brain networks (2024), pages:

2024.07.22.604675 Section: New Results.

[52] R. Herzog, F. E. Rosas, R. Whelan, S. Fittipaldi, H. Santamaria-Garcia, J. Cruzat, A. Birba, S. Moguilner, E. Tagliazucchi, P. Prado, and A. Ibanez, enGenuine high-order interactions in brain networks and neurodegeneration, Neurobiology of Disease **175**, 105918 (2022).

[53] H. Wang, Y. Liu, and Y. Ding, enIdentifying Diagnostic Biomarkers for Autism Spectrum Disorder From Higher-order Interactions Using the PED Algorithm, Neuroinformatics 10.1007/s12021-024-09662-w (2024).

[54] Q. Li, V. D. Calhoun, A. R. Ballem, S. Yu, J. Malo, and A. Iraji, Aberrant High-Order Dependencies in Schizophrenia Resting-State Functional MRI Networks (2023), arXiv:2310.17445 [q-bio].

[55] I. Pirovano, Y. Antonacci, A. Mastropietro, C. Barà, L. Sparacino, E. Guanziroli, F. Molteni, M. Tettamanti, L. Faes, and G. Rizzo, Rehabilitation Modulates High-Order Interactions Among Large-Scale Brain Networks in Subacute Stroke, IEEE Transactions on Neural Systems and Rehabilitation Engineering **31**, 4549 (2023), conference Name: IEEE Transactions on Neural Systems and Rehabilitation Engineering.

[56] F. Zamani Esfahlani, Y. Jo, J. Faskowitz, L. Byrge, D. P. Kennedy, O. Sporns, and R. F. Betzel, High-amplitude cofluctuations in cortical activity drive functional connectivity, Proceedings of the National Academy of Sciences **117**, 28393 (2020), publisher: Proceedings of the National Academy of Sciences.

[57] A. Santoro, F. Battiston, G. Petri, and E. Amico, enHigher-order organization of multivariate time series, Nature Physics , 1 (2023), publisher: Nature Publishing Group.

[58] J. C. Tanner, J. Faskowitz, L. Byrge, D. P. Kennedy, O. Sporns, and R. F. Betzel, enSynchronous high-amplitude co-fluctuations of functional brain networks during movie-watching (2022), pages: 2022.06.30.497603 Section: New Results.

[59] R. Betzel, S. Cutts, J. Tanner, S. Greenwell, T. Varley, J. Faskowitz, and O. Sporns, Hierarchical organization of spontaneous co-fluctuations in densely-sampled individuals using fMRI, bioRxiv (2022), publisher: Cold Spring Harbor Laboratory.

[60] D. Balduzzi and G. Tononi, engIntegrated information in discrete dynamical systems: motivation and theoretical framework, PLoS computational biology **4**, e1000091 (2008).

[61] A. I. Luppi, P. A. M. Mediano, F. E. Rosas, J. Allanson, J. D. Pickard, G. B. Williams, M. M. Craig, P. Finoia, A. R. D. Peattie, P. Coppola, D. K. Menon, D. Bor, and E. A.

Stamatakis, enReduced emergent character of neural dynamics in patients with a disrupted connectome, NeuroImage **269**, 119926 (2023).

[62] A. I. Luppi, P. A. M. Mediano, F. E. Rosas, J. Allanson, J. D. Pickard, R. L. Carhart-Harris, G. B. Williams, M. M. Craig, P. Finoia, A. M. Owen, L. Naci, D. K. Menon, D. Bor, and E. A. Stamatakis, enA Synergistic Workspace for Human Consciousness Revealed by Integrated Information Decomposition, eLife **12**, 10.7554/eLife.88173.2 (2024), publisher: eLife Sciences Publications Limited.

[63] M. Wenzel, S. Han, E. H. Smith, E. Hoel, B. Greger, P. A. House, and R. Yuste, Reduced Repertoire of Cortical Microstates and Neuronal Ensembles in Medically Induced Loss of Consciousness, Cell Systems 10.1016/j.cels.2019.03.007 (2019).

[64] O. M. Cliff, L. Novelli, B. D. Fulcher, J. M. Shine, and J. T. Lizier, Assessing the significance of directed and multivariate measures of linear dependence between time series, Physical Review Research **3**, 013145 (2021), publisher: American Physical Society.

[65] F. Váša and B. Mišić, enNull models in network neuroscience, Nature Reviews Neuroscience **23**, 493 (2022), publisher: Nature Publishing Group.

[66] A. Schaefer, R. Kong, E. M. Gordon, T. O. Laumann, X.-N. Zuo, A. J. Holmes, S. B. Eickhoff, and B. T. T. Yeo, engLocal-Global Parcellation of the Human Cerebral Cortex from Intrinsic Functional Connectivity MRI, Cerebral Cortex (New York, N.Y.: 1991) **28**, 3095 (2018).

[67] L. G. S. Jeub, O. Sporns, and S. Fortunato, engMultiresolution Consensus Clustering in Networks, Scientific Reports **8**, 3259 (2018).

[68] J. Faskowitz, F. Z. Esfahlani, Y. Jo, O. Sporns, and R. F. Betzel, enEdge-centric functional network representations of human cerebral cortex reveal overlapping system-level architecture, Nature Neuroscience **23**, 1644 (2020), number: 12 Publisher: Nature Publishing Group.

[69] U. Fano, Ionization Yield of Radiations. II. The Fluctuations of the Number of Ions, Physical Review **72**, 26 (1947), publisher: American Physical Society.

[70] R. G. James, C. J. Ellison, and J. P. Crutchfield, Anatomy of a bit: Information in a time series observation, Chaos: An Interdisciplinary Journal of Nonlinear Science **21**, 037109 (2011), publisher: American Institute of Physics.

[71] F. Rosas, P. A. M. Mediano, M. Gastpar, and H. J. Jensen, Quantifying High-order Interdependencies via Multivariate Extensions of the Mutual Information, Physical Review E **100**, 032305 (2019), number: 3 arXiv: 1902.11239.

[72] S. Watanabe, Information Theoretical Analysis of Multivariate Correlation, IBM Journal of Research and Development **4**, 66 (1960), number: 1.

[73] S. A. Abdallah and M. D. Plumbley, enA measure of statistical complexity based on predictive information with application to finite spin systems, Physics Letters A **376**, 275 (2012).

[74] T. F. Varley and P. Kaminski, enUntangling Synergistic Effects of Intersecting Social Identities with Partial Information Decomposition, Entropy **24**, 1387 (2022), number: 10 Publisher: Multidisciplinary Digital Publishing Institute.

[75] A. E. Goodwell and P. Kumar, enTemporal Information Partitioning Networks (TIPNets): A process network approach to infer ecohydrologic shifts, Water Resources Research **53**, 5899 (2017), _eprint: https://onlinelibrary.wiley.com/doi/pdf/10.1002/2016WR020218.

[76] A. E. Goodwell, P. Jiang, B. L. Ruddell, and P. Kumar, enDebates—Does Information Theory Provide a New Paradigm for Earth Science? Causality, Interaction, and Feedback, Water Resources Research **56**, e2019WR024940 (2020), _eprint: https://onlinelibrary.wiley.com/doi/pdf/10.1029/2019WR024940.

[77] H. Rajpal and O. A. Guerrero, enSynergistic Small Worlds that Drive Technological Sophistication (2023).

[78] D. Marinazzo, J. Van Roozendaal, F. E. Rosas, M. Stella, R. Comolatti, N. Colenbier, S. Stramaglia, and Y. Rosseel, engAn information-theoretic approach to build hypergraphs in psychometrics, Behavior Research Methods 10.3758/s13428-024-02471-8 (2024).

[79] D. Marinazzo, L. Angelini, M. Pellicoro, and S. Stramaglia, Synergy as a warning sign of transitions: The case of the two-dimensional Ising model, Physical Review E **99**, 040101 (2019), publisher: American Physical Society.

[80] T. Scagliarini, D. Marinazzo, Y. Guo, S. Stramaglia, and F. E. Rosas, Quantifying high-order interdependencies on individual patterns via the local O-information: Theory and applications to music analysis, Physical Review Research **4**, 013184 (2022), publisher: American Physical Society.

[81] G. Tononi, O. Sporns, and G. M. Edelman, enA measure for brain complexity: relating functional segregation and integration in the nervous system, Proceedings of the National Academy of Sciences **91**, 5033 (1994), number: 11.

[82] P. A. M. Mediano, F. E. Rosas, J. C. Farah, M. Shanahan, D. Bor, and A. B. Barrett, Integrated information as a common signature of dynamical and information-processing complex-

ity, Chaos: An Interdisciplinary Journal of Nonlinear Science **32**, 013115 (2022), publisher: American Institute of Physics.

[83] P. A. M. Mediano, F. E. Rosas, A. I. Luppi, R. L. Carhart-Harris, D. Bor, A. K. Seth, and A. B. Barrett, Towards an extended taxonomy of information dynamics via Integrated Information Decomposition, arXiv:2109.13186 [physics, q-bio] (2021), arXiv: 2109.13186.

[84] M. P. van den Heuvel, S. C. de Lange, A. Zalesky, C. Seguin, B. T. T. Yeo, and R. Schmidt, enProportional thresholding in resting-state fMRI functional connectivity networks and consequences for patient-control connectome studies: Issues and recommendations, NeuroImage **152**, 437 (2017).

[85] M. Levin, engBioelectric networks: the cognitive glue enabling evolutionary scaling from physiology to mind, Animal Cognition **26**, 1865 (2023).

[86] M. Levin, EnglishThe Computational Boundary of a "Self": Developmental Bioelectricity Drives Multicellularity and Scale-Free Cognition, Frontiers in Psychology **10**, 10.3389/fpsyg.2019.02688 (2019), publisher: Frontiers.

[87] A. S. Reber and F. Baluška, engCognition in some surprising places, Biochemical and Biophysical Research Communications **564**, 150 (2021).

[88] M. Pope, M. Fukushima, R. F. Betzel, and O. Sporns, Modular origins of high-amplitude cofluctuations in fine-scale functional connectivity dynamics, Proceedings of the National Academy of Sciences **118**, e2109380118 (2021), publisher: Proceedings of the National Academy of Sciences.

[89] M. Pope, C. Seguin, T. F. Varley, J. Faskowitz, and O. Sporns, enCo-evolving dynamics and topology in a coupled oscillator model of resting brain function, NeuroImage **277**, 120266 (2023).

[90] S. Sisakhtnezhad and L. Khosravi, Emerging physiological and pathological implications of tunneling nanotubes formation between cells, European Journal of Cell Biology **94**, 429 (2015).

[91] C. R. Zaccard, C. R. Rinaldo, and R. B. Mailliard, Linked in: immunologic membrane nanotube networks, Journal of Leukocyte Biology **100**, 81 (2016).

[92] M. Dupont, S. Souriant, G. Lugo-Villarino, I. Maridonneau-Parini, and C. Vérollet, EnglishTunneling Nanotubes: Intimate Communication between Myeloid Cells, Frontiers in Immunology **9**, 10.3389/fimmu.2018.00043 (2018), publisher: Frontiers.

[93] S. Abounit and C. Zurzolo, Wiring through tunneling nanotubes – from electrical signals to organelle transfer, Journal of Cell Science **125**, 1089 (2012).

[94] S. Gurung, D. Perocheau, L. Touramanidou, and J. Baruteau, The exosome journey: from biogenesis to uptake and intracellular signalling, Cell Communication and Signaling **19**, 47 (2021).

[95] M. Gatica, F. E. Rosas, P. A. M. Mediano, I. Diez, S. P. Swinnen, P. Orio, R. Cofré, and J. M. Cortes, enHigh-order functional redundancy in ageing explained via alterations in the connectome in a whole-brain model, PLOS Computational Biology **18**, e1010431 (2022), publisher: Public Library of Science.

[96] C. Stringer, T. Wang, M. Michaelos, and M. Pachitariu, enCellpose: a generalist algorithm for cellular segmentation, Nature Methods **18**, 100 (2021), publisher: Nature Publishing Group.

[97] D. C. Van Essen, S. M. Smith, D. M. Barch, T. E. J. Behrens, E. Yacoub, and K. Ugurbil, enThe WU-Minn Human Connectome Project: An overview, NeuroImage Mapping the Connectome, **80**, 62 (2013).

[98] G. T. Cantwell, Y. Liu, B. F. Maier, A. C. Schwarze, C. A. Serván, J. Snyder, and G. St-Onge, Thresholding normally distributed data creates complex networks, Physical Review E **101**, 062302 (2020), number: 6 Publisher: American Physical Society.

[99] T. Adamovich, I. Zakharov, A. Tabueva, and S. Malykh, enThe thresholding problem and variability in the EEG graph network parameters, Scientific Reports **12**, 18659 (2022), number: 1 Publisher: Nature Publishing Group.

[100] V. A. Traag and J. Bruggeman, Community detection in networks with positive and negative links, Physical Review E **80**, 036115 (2009), publisher: American Physical Society.

[101] S. Fortunato and M. Barthélemy, enResolution limit in community detection, Proceedings of the National Academy of Sciences **104**, 36 (2007), number: 1.

[102] A. Lancichinetti and S. Fortunato, enConsensus clustering in complex networks, Scientific Reports **2**, 336 (2012), number: 1 Publisher: Nature Publishing Group.

[103] M. E. J. Newman and M. Girvan, Finding and evaluating community structure in networks, Physical Review E **69**, 026113 (2004), publisher: American Physical Society.

[104] V. Traag, vtraag/libleidenalg (2024), original-date: 2022-11-28T21:16:48Z.

[105] T. F. Varley and O. Sporns, Network Analysis of Time Series: Novel Approaches to Network Neuroscience, Frontiers in Neuroscience **15** (2022).

[106] T. F. Varley, enGeneralized decomposition of multivariate information, PLOS ONE **19**, e0297128 (2024), publisher: Public Library of Science.

[107] N. M. Timme, N. J. Marshall, N. Bennett, M. Ripp, E. Lautzenhiser, and J. M. Beggs, EnglishCriticality Maximizes Complexity in Neural Tissue, Frontiers in Physiology **7**, 10.3389/fphys.2016.00425 (2016).

[108] G. Tononi and O. Sporns, enMeasuring information integration, BMC Neuroscience **4**, 31 (2003), number: 1.

[109] B. W. Kernighan and S. Lin, An efficient heuristic procedure for partitioning graphs, The Bell System Technical Journal **49**, 291 (1970), conference Name: The Bell System Technical Journal.

[110] A. A. Hagberg, D. A. Schult, and P. J. Swart, Exploring Network Structure, Dynamics, and Function using NetworkX, in *Proceedings of the 7th Python in Science Conference*, edited by G. Varoquaux, T. Vaught, and J. Millman (Pasadena, CA USA, 2008) pp. 11 – 15.

[111] T. F. Varley and J. Bongard, Evolving higher-order synergies reveals a trade-off between stability and information-integration capacity in complex systems, Chaos: An Interdisciplinary Journal of Nonlinear Science **34**, 063127 (2024).